Available online at www.sciencedirect.com
ScienceDirect
Catalysis Today 129 (2007) 118–126
CATALYSIS TODAY
www.elsevier.com/locate/cattod

Optimal design and modeling of annular photocatalytic wall reactors

Gustavo E. Imoberdorf, Alberto E. Cassano, Horacio A. Irazoqui, Orlando M. Alfano *

INTEC, Instituto de Desarrollo Tecnológico para la Industria Química, Universidad Nacional del Litoral and CONICET, Güemes 3450, S3000GLM Santa Fe, Argentina

Available online 6 August 2007

Abstract

The performance of photocatalytic reactors is largely conditioned by their configuration. In particular, photocatalytic wall reactors are affected by configuration-linked factors such as diffusive resistances, reactor radiation incidence and absorption efficiencies, and by the amount of photocatalytic surface area that is effectively irradiated. In this paper, the effect of different configurations and design variables on the performance of annular photocatalytic reactors was analyzed. With this purpose, a complete reactor model was developed and solved, taking into account single- and multi-annular configurations, different reactor dimensions, and three flow patterns. The model was successfully validated against experimental results for the photocatalytic oxidation of perchloroethylene (PCE) in a multi-annular reactor. From the simulation results, it was possible to conclude that the unfavorable effect of the diffusive resistances on the reactor performance could be reduced by constructing photocatalytic annular wall reactors of small annular width and large photocatalytic surface area. Besides, the multi-annular configuration is more effective in using the radiative energy fed into the reactor than the single-annulus reactor configuration. According to the results obtained for PCE photocatalytic degradation, among all the studied reactor configurations the most efficient one is that with its annuli interconnected in a series pattern.

Keywords: Photocatalysis; Optimal design; Modeling; Air pollution remediation; Multi-annular photocatalytic reactor

1. Introduction

Photocatalysis has been proven to be an effective means to remove pollutants from water and air [1–4]. However, the application of photocatalytic technologies for pollutants degradation at a commercial scale is currently hindered, among other factors, by a lack of physically based mathematical models that can be used for reactor design and optimization. It has been shown that annular photocatalytic wall reactors are efficient at eliminating volatile organic compounds (VOCs) from air streams [5–11]. The performance of this type of reactors may be increased by properly choosing their geometrical dimensions and flow pattern. The criterion of optimal reactor design used in this work consists in searching for the maximum pollutant conversion by changing the reactor configuration and its geometrical dimensions, while keeping the operating conditions invariant, for the same pollutant compound and UV lamp characteristics.

Optimal design is closely related to both modeling and simulation. Indeed, these computational tools are almost essential to analyze the effect of the reactor design variables on the results of the process (i.e. the reactor conversion). Important contributions to the modeling of photocatalytic reactors for the degradation of gaseous pollutants have been published [7,12–14].

Jacoby et al. [15] studied that the kinetics of trichloroethylene oxidation in gas phase in an annular photocatalytic reactor. They experimentally showed the existence of a bulk-transport-control regime. Mass transport limitations could be reduced by operating with high volumetric flow rates. Based on computational fluid dynamics (CFD), Mohseni and Taghipour [16] presented a complete analysis of the flow characteristics and its impact on the overall destruction of gas phase contaminants in a photocatalytic annular reactor. They used vinyl chloride as a model pollutant. Important diffusive resistance and flow short circuiting were identified from model results. Frequently, these two problems negatively impact on the performance of photocatalytic reactors, providing significant driving and motivation for optimization. Along the same lines, Shiraishi et al. [10] indicated that diffusional resistances generally reduce

* Corresponding author. Tel.: +54 342 451 1546/47; fax: +54 342 451 1087.
E-mail address: alfano@intec.unl.edu.ar (O.M. Alfano).

0920-5861/$ – see front matter © 2007 Elsevier B.V. All rights reserved.
doi:10.1016/j.cattod.2007.06.057

the efficiencies of photocatalytic reactors, particularly when low pollutant concentrations are used.

Despite that some contributions on photocatalytic reactor modeling have been published, to the best of our knowledge no optimal design applied to annular photocatalytic wall reactors has been proposed. The objective of the present work is to analyze the effect of reactor design variables and configuration on the pollutant degradation efficiency. For this, perchloroethylene (PCE) was used as the model pollutant. The present article comprises of four sections. In the first one, we describe six different photocatalytic reactor configurations: three of the single-annulus type and three multi-annular reactors. Different configuration parameters were chosen with the objective of identifying the effect of the reactor physical design on its performance. In the second section, a complete mathematical model developed to predict the pollutant conversion is present. This mathematical model takes into account the concurrent phenomena of mass, momentum and radiative energy transfer. The third section is devoted to the presentation and discussion of the predicted pollutant conversions achieved in each reactor. Finally, the experimental validation process of the model is presented. To do that, we built one of the proposed reactor configurations: the multi-annular reactor operated with a series flow pattern.

2. Description of the annular photocatalytic wall reactor configurations

Different single- and multi-annular photocatalytic reactor configurations have been analyzed by means of a complete mathematical model. These reactor configurations consist of two or more concentric cylindrical borosilicate glass tubes which are transparent to UV radiation (Fig. 1). In each case, the UV radiation is supplied by a tubular UV lamp (Philips TL 18 W) placed at each reactor central axis. The concentric borosilicate glass tubes give rise either to a single annular space (reactors A–C) or to three annular spaces (reactors D–F). The polluted air carrying reactants and products flows through these annular spaces. The tube walls are directly in contact with the polluted gas phase and were covered with thin layers of TiO_2. The dimensions of each reactor are shown in Table 1. In order to maximize the usage of the radiative energy emitted by the lamp, the maximum reactor length compatible with the employed UV lamp was chosen in all cases (reactors A–F). Perchloroethylene (PCE) was used as model air pollutant.

Regarding the single-annular photocatalytic reactor configuration, it was analyzed that the effect on the pollutant conversion of: (i) the reactor volume (proportional to the contaminated air residence time in the reactor for a given flow rate); (ii) the photocatalytic area; and (iii) the annulus width. Three single-annular reactors were considered (reactors A–C) and their dimensions were chosen so as to stress the effect of the reactor physical design on its performance under the same operating conditions. The physical characteristics of these single-annular reactors are:

- *Reactor A*. Single-annular photocatalytic reactor with a comparatively large volume ($V = 2178\ cm^3$, $A = 1718\ cm^2$, and $R_{ext} - R_{int} = 2.5$ cm).
- *Reactor B*. Single-annular photocatalytic reactor with a comparatively small volume and small photocatalytic surface area ($V = 633\ cm^3$, $A = 1266\ cm^2$, and $R_{ext} - R_{int} = 1$ cm).
- *Reactor C*. Single-annular photocatalytic reactor with comparatively small volume and large photocatalytic surface area ($V = 1085\ cm^3$, $A = 2170\ cm^2$, and $R_{ext} - R_{int} = 1$ cm).

The performance of multi-annular reactors was also studied. This reactor configuration improves the radiative energy absorption, because the radiation transmitted through the two TiO_2 films of the inner annulus can be absorbed by the TiO_2 films of the middle and outer annuli. When all the TiO_2 films covering the tube walls of the multi-annular reactor have the same thickness, the value of the superficial rate of photon absorption decreases significantly from the inner to the middle and the outer annuli, mainly as a consequence of the radiative energy attenuation caused by the absorbing medium (TiO_2). This non-uniformity of the rate of photon absorption has an important effect on the reactor performance. In the case of multi-annular reactor configurations, the effect on the reactor conversion of (i) the type of flow pattern (either series or

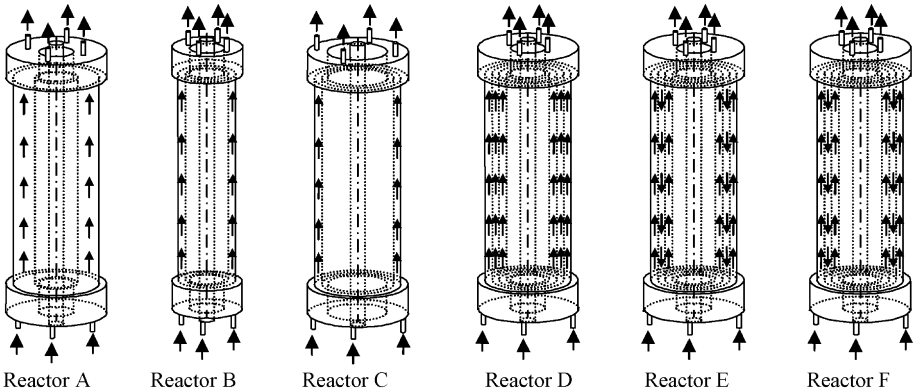

Fig. 1. Photocatalytic reactors. Keys: (A) single-annular reactor with high residence time; (B and C) single-annular reactor with low residence time; (D) multi-annular parallel flow reactor; (E) multi-annular series flow reactor (each annular channel wall coated with TiO_2 film of uniform thickness); (F) multi-annular series flow reactor (superficial rate of photon absorption uniformly distributed on the active surfaces).

Table 1
Single- and multi-annular reactor dimensions and operating conditions

	Reactor A	Reactor B	Reactor C	Reactors D, E, and F
Inner and outer radii of the reactor annuli (cm)	1.6–4.1	1.6–2.6	3.1–4.1	1.7–2.3, 2.5–3.3, 3.5–4
Reactor length (cm)	48	48	48	48
Volume of the reactor (cm^3)	2178	633	1085	1600
Photocatalytic active area (cm^2)	1718	1266	2170	5208
η_I (%)	82.5	82.5	82.4	82.5
η_A (%)	80.1	79.9	77.1	92
η_R (%)	0.28	0.33	0.39	0.26, 0.33, and 0.34
Residence time (s)	21.8	6.3	10.9	16
Operating conditions	Volumetric gas flow rate = 100 $cm^3\ s^{-1}$; relative humidity = 50%; $C^{in}_{PCE} = 50$ ppm; $T = 25\ ^\circ C$; $P = 1$ atm; radiation source: Philips TL UV lamp, and 18 W without optical filters.			

parallel) and (ii) the thickness distribution among the TiO_2 films deposited on the concentric tubes, were analyzed. Three multi-annular reactors were considered:

- *Reactor D*. Multi-annular reactor with parallel flow pattern and uniform thickness of TiO_2 films. The total volumetric flow rate of the feed stream was divided among the three annular channels, in such a way that the flow rate in each channel was proportional to the corresponding annular cross section.
- *Reactor E*. Multi-annular reactor with series flow pattern and a single uniform thickness of all the TiO_2 films.
- *Reactor F*. Multi-annular reactor with series flow pattern and a single value of the photon absorption rate for all the TiO_2 films (this condition was achieved by choosing different TiO_2 film thicknesses, depending on the tube considered).

It should be noted that the external dimensions of the three multi-annular reactors are the same (Table 1), but they operate with different flow patterns or they have different distribution of UV absorption rates (uniform/non-uniform).

3. Mathematical modeling of the proposed reactors

A 2D mass balance was developed taking into account the intrinsic kinetics of the pollutant model (PCE), as well as the mass transfer rate processes and the absorption of radiative energy. The following assumptions were made [11]: (i) reactor operating under steady state; (ii) fully developed laminar flow; (iii) Newtonian fluid; (iv) azimuthal symmetry; (v) diffusive mass flow in the axial direction negligible when compared with convective flow; (vi) chemical reactions take place only on the photocatalytic films; (vii) constant physical properties; (viii) TiO_2 coatings are always thin enough so that they can be considered two-dimensional films offering no internal resistances to mass transfer. Under these conditions, the differential mass transfer equation for PCE can be written as

$$\frac{\partial C_{PCE}(r,z)}{\partial z} V_{z,j}(r) = \frac{D^0_{PCE-Air}}{r} \frac{\partial}{\partial r}\left(r \frac{\partial C_{PCE}(r,z)}{\partial r}\right); \quad (0 < z < Z_R;\ \ \chi_j R_j < r < R_j) \tag{1}$$

with the boundary conditions:

$$D^0_{PCE-Air} \left.\frac{\partial C_{PCE}(r,z)}{\partial r}\right|_{r=R_j} = r_{PCE}(R_j, z); \quad (0 < z < Z_R) \tag{2}$$

$$D^0_{PCE-Air} \left.\frac{\partial C_{PCE}(r,z)}{\partial r}\right|_{r=\chi_j R_j} = -r_{PCE}(\chi_j R_j, z) \quad (0 < z < Z_R) \tag{3}$$

where C_{PCE} is the local PCE concentration, $D^0_{PCE-Air}$ the molecular diffusion coefficient of PCE in air ($D^0_{PCE-Air} = 0.072\ cm^2\ s^{-1}$), and $r_{PCE}(\chi_j R_j, z)$ and $r_{PCE}(R_j, z)$ are the PCE local reaction rates on the catalytic surface of the inner and outer wall of each annular channel, respectively. The rate of the pollutant degradation reaction (r_{PCE}) depends on the PCE concentration in gas phase at contact with the photocatalytic surface; on the relative humidity; and on the superficial rate of photon absorption. Subscript j equals 1 for reactors A–C, and it runs from 1 to 3 for reactors D–F, as it discriminates among the inner, middle and outer annular channels.

Besides, for reactors A–C, the PCE concentration at the reactor inlet is given by

$$C_{PCE}(r,z)|_{z=0} = C^{in}_{PCE}; \quad (\chi_1 R_1 < r < R_1) \tag{4}$$

and for the same reactors, the outlet PCE concentration is calculated as follows

$$C^{out}_{PCE} = \frac{\int_{\chi_1 R_1}^{R_1} C_{PCE}(r, Z_R) V_{z,1}(r) r dr}{\int_{\chi_1 R_1}^{R_1} V_{z,1}(r) r dr} \tag{5}$$

The multi-annular reactor D operates with parallel flow pattern; thus, the PCE concentration at the inlet of each channel is

$$C_{PCE}(r,z)|_{z=0} = C^{in}_{PCE}; \quad (\chi_i R_i < r < R_i); \ \ (j = 1,2,3) \tag{6}$$

and the outlet PCE concentration is given by

$$C^{out}_{PCE} = \frac{\sum_{j=1}^{3} \int_{\chi_j R_j}^{R_j} C_{PCE}(r, Z_R) V_{z,j}(r) r\, dr}{\sum_{j=1}^{3} \int_{\chi_j R_j}^{R_j} V_{z,j}(r) r\, dr} \tag{7}$$

For the multi-annular reactors E and F, operating with a series flow pattern, the PCE concentrations at the inlet of each annular

channel are

$$C_{\mathrm{PCE}}(r,z)|_{z=0} = C_{\mathrm{PCE}}^{\mathrm{in}}; \quad (\chi_3 R_3 < r < R_3) \tag{8}$$

$$C_{\mathrm{PCE}}(r,z)\Big|_{z=Z_{\mathrm{R}}} = \frac{\int_{k_3R_3}^{R_3} C_{\mathrm{PCE}}(r,Z_{\mathrm{R}})V_{z,3}(r)r\,\mathrm{d}r}{\int_{k_3R_3}^{R_3} V_{z,3}(r)r\,\mathrm{d}r}; \quad (\chi_2 R_2 < r < R_2) \tag{9}$$

$$C_{\mathrm{PCE}}(r,z)\Big|_{z=0} = \frac{\int_{k_2R_2}^{R_2} C_{\mathrm{PCE}}(r,0)V_{z,2}(r)r\,\mathrm{d}r}{\int_{k_2R_2}^{R_2} V_{z,2}(r)r\,\mathrm{d}r}; \quad (\chi_1 R_1 < r < R_1) \tag{10}$$

and the outlet PCE concentration is

$$C_{\mathrm{PCE}}^{\mathrm{out}} = \frac{\int_{\chi_1R_1}^{R_1} C_{\mathrm{PCE}}(r,Z_{\mathrm{R}})V_{z,1}(r)r\,\mathrm{d}r}{\int_{\chi_1R_1}^{R_1} V_{z,1}(r)r\,\mathrm{d}r} \tag{11}$$

The value of the PCE conversion for all the reactor configurations (A–F) is given by

$$X_{\mathrm{PCE}} = \frac{C_{\mathrm{PCE}}^{\mathrm{in}} - C_{\mathrm{PCE}}^{\mathrm{out}}}{C_{\mathrm{PCE}}^{\mathrm{in}}} \times 100 \tag{12}$$

For reactor configurations A, B, C, E, and F, the fully developed velocity profile for a laminar flow of a Newtonian fluid through the jth annular duct is

$$V_{z,j}(r) = (-1)^{j+1}\frac{2Q}{\pi R_j^2}\frac{\ln\chi_j}{(1-\chi_j^4)\ln\chi_j + (1-\chi_j^2)^2}\left[1-\left(\frac{r}{R_j}\right)^2 - \frac{1-\chi_j^2}{\ln\chi_j}\ln\left(\frac{r}{R_j}\right)\right] \tag{13}$$

whereas for reactor D, the flow rate through each channel is proportional to the annular cross section of the corresponding channel, and consequently:

$$V_{z,j}(r) = \frac{2Q(1-\chi_j^2)}{\pi\sum_{k=1}^{3}(R_k^2-\chi_k^2R_k^2)}\frac{\ln\chi_j}{(1-\chi_j^4)\ln\chi_j + (1-\chi_j^2)^2}\left[1-\left(\frac{r}{R_j}\right)^2 - \frac{1-\chi_j^2}{\ln\chi_j}\ln\left(\frac{r}{R_j}\right)\right] \tag{14}$$

The PCE local reaction rate on the catalytic surface of the inner and outer wall of each annular channel enters the model through the boundary conditions (Eqs. (2) and (3)). In a previous work [17], the degradation kinetics of PCE from a moist air stream was studied for different values of PCE feed concentrations, relative humidities, and irradiation levels in a differential flat-plate reactor without mass transfer limitations. This kinetic model was derived from a plausible reaction mechanism [18–21]. For the experimental conditions used, the local PCE reaction rate was found to be

$$r_{\mathrm{PCE}}(r,z) = -\alpha\frac{C_{\mathrm{PCE}}(r,z)}{1+K_{\mathrm{H_2O}}C_{\mathrm{H_2O}}}e^{\mathrm{a,s}}(r,z) \tag{15}$$

where $e^{\mathrm{a,s}}(r,z)$ is the local superficial rate of photon absorption (or LSRPA) and α and $K_{\mathrm{H_2O}}$ are the kinetic parameters that were regressed from experimental data using the Levenberg–Marquardt method. The obtained parameter values are: $\alpha = 1.54\times10^{8}\ \mathrm{cm^3\ Einstein^{-1}}$ and $K_{\mathrm{H_2O}} = 3.21\times10^{-4}\ \mathrm{m^3\ mg^{-1}}$. It should be noted that the kinetic expression of Eq. (15) shows: (1) first order with respect to the PCE concentration; (2) linear dependence with respect to the local photon absorption rate ($e^{\mathrm{a,s}}$); and (3) site-competitive adsorption between PCE and water, resulting in a direct dependence of the kinetics on the relative humidity.

The mean value of the pollutant reaction rate on the reactor catalytic surface is

$$\left\langle r_{\mathrm{PCE}}\right\rangle_{\mathrm{AR}} = \frac{\int_{A_{\mathrm{R}}} r_{\mathrm{PCE}}(r,z)\mathrm{d}A}{A_{\mathrm{R}}} \tag{16}$$

where A_{R} is the active catalytic surface area.

$$A_{\mathrm{R}} = \sum_{j=1}^{n} 2\pi(\chi_j R_j + R_j)L_{\mathrm{R}} \tag{17}$$

In Eq. (17), $n = 1$ for reactors A–C and $n = 3$ for reactors D–F, while L_{R} is the reactor length.

A radiation field model was developed to predict the LSRPA at each point on the photocatalytic films [11]. These values are needed to calculate the local reaction rate (Eq. (15)). In order to compute the UV radiation field we adopted the three-dimensional source with superficial emission model [22] and the ray-tracing computational method. The spectral local superficial rate of photon absorption ($e_{\lambda}^{a,s}$) at each point on the reactor catalytic walls is given by

$$e_{\lambda}^{\mathrm{a,s}}(r,z) = \int_{\phi_{\min}(r)}^{\phi_{\max}(r)}\int_{\theta_{\min}(r,z,\phi)}^{\theta_{\max}(r,z,\phi)}\frac{P_{\lambda,\mathrm{L}}}{2\pi^2R_{\mathrm{L}}Z_{\mathrm{L}}}\exp\left(-n_{\mathrm{g}}(r)\frac{\kappa_{\lambda,\mathrm{g}}e_{\mathrm{g}}}{\cos\alpha_{\mathrm{n}}} - n_{\mathrm{f}}(r)\frac{\kappa_{\lambda,\mathrm{f}}e_{\mathrm{f}}}{\cos\alpha_{\mathrm{n}}}\right)\left[1-\exp\left(-\frac{\kappa_{\lambda,\mathrm{f}}e_{\mathrm{f}}}{\cos\alpha_{\mathrm{n}}}\right)\right]\cos\phi\sin^2\theta\,\mathrm{d}\theta\,\mathrm{d}\phi \tag{18}$$

where $\kappa_{\lambda,\mathrm{f}}$ and $\kappa_{\lambda,\mathrm{g}}$ are the spectral absorption coefficients of the TiO_2 film and of the glass tubes, e_{f} and e_{g} are their corresponding thicknesses, α_{n} the angle between the ray trajectory and the film outwardly directed normal, and n_{g} and n_{f} are the number of times that a radiation beam has been attenuated by a glass tube wall or by a TiO_2 film, respectively, before its incidence at the (r,z) position on the catalytic surface. Besides, $P_{\lambda,\mathrm{L}}$ is the spectral emission power of the lamp, and R_{L} and Z_{L} are the radius and length of the lamp, respectively.

To obtain the LSRPA we have to add up all the contributions $e_{\lambda}^{\mathrm{a,s}}(r,z)$ resulting from the lamp spectral emission distribution, that fall in the range of wavelengths of interest (300–420 nm):

$$e^{\mathrm{a,s}}(r,z) = \sum_{\lambda=300\,\mathrm{nm}}^{420\,\mathrm{nm}} e_{\lambda}^{\mathrm{a,s}}(r,z) \tag{19}$$

The average value of the LSRPA on the reactor catalytic surface area (A_{R}), or the surface rate of photon absorption (SRPA), is

defined as follows

$$\left\langle e^{a,s} \right\rangle_{A_R} = \frac{\sum_{\lambda=300\,nm}^{420\,nm} \int_{A_R} e^{a,s}(r,z)\,dA}{A_R} \quad (20)$$

Another property that is necessary for the radiation model calculations is the spectral net radiative flux on the area of the reactor wall of radiation entrance, given by

$$q_{\lambda,RW} = \int_{\phi_{min}(R_W)}^{\phi_{max}(R_W)} \int_{\theta_{min}(R_W,z,\phi)}^{\theta_{max}(R_W,z,\phi)} \frac{P_{\lambda,L}}{2\pi^2 R_L Z_L} \cos\phi \sin^2\theta \, d\theta \, d\phi \quad (21)$$

The total quantum efficiency (η_T) was employed to compare how well photocatalytic reactors make use of the energy emitted by the lamp to decompose the pollutant. This efficiency is defined as the ratio of the number of molecules of the pollutant reacted to the number of photons emitted by the lamp. The total quantum efficiency can be expressed as the product of the reactor radiation incidence efficiency (η_I), the catalyst radiation absorption efficiency (η_A), and the overall reaction quantum efficiency (η_R) [23]:

$$\eta_T = \eta_I \eta_A \eta_R \quad (22)$$

The reactor radiation incidence efficiency (η_I) is the ratio of photons entering the reactor to the total number of photons emitted by the lamp. It can be obtained as follows

$$\eta_I = \frac{\int_{A_{RW}} \int_{\lambda_L} q_{\lambda,RW}\,d\lambda\,dA}{\int_{\lambda_L} P_{\lambda,L}\,d\lambda} \quad (23)$$

where A_{RW} is the area of radiation entrance to the reactor (i.e. the inside wall of the inner tube) and $q_{\lambda,RW}$ is obtained from Eq. (21). The value of η_I depends on the reactor-lamp configuration and dimensions and on the optical properties of its building materials.

The catalyst radiation absorption efficiency (η_A) is the fraction of photons that entered the reactor, are absorbed by the catalytic films. The numerical values of η_A can be obtained by

$$\eta_A = \frac{\int_{A_R} \int_{\lambda_L} e_\lambda^{a,s}\,d\lambda\,dA}{\int_{A_{RW}} \int_{\lambda_L} q_{\lambda,RW}\,d\lambda\,dA} \quad (24)$$

This efficiency depends on the optical properties of the reactor building materials (mainly the photocatalyst optical properties) and on the internal reactor configuration. For the reactors considered in this work, the TiO_2 catalyst is immobilized on the tube walls in contact with the fluid streams. After entering the reactor, part of the UV radiation is partially absorbed by the thin TiO_2 catalytic films; a small part is absorbed by the borosilicate tubes, and the rest is transmitted through the films or reflected on their surface. However, only the radiative energy absorbed by the TiO_2 films is useful for the pollutant degradation reaction. The radiation absorption efficiency η_A takes into account the reduction of the radiative energy available for the reaction due to these effects.

Finally, the overall reaction quantum efficiency (η_R) is defined as the ratio of the number of molecules of PCE reacted to the number of photons absorbed by the catalytic film. This efficiency can be obtained by

$$\eta_R = -\frac{\left\langle r_{PCE} \right\rangle_{AR}}{\left\langle e^{a,s} \right\rangle_{AR}} \quad (25)$$

The value of η_R depends on the specific reaction taking place as well as on the nature of the photocatalyst employed and is strongly affected by the reactor operating conditions. Only under uniquely defined conditions, its value is useful to compare different reacting systems and reactor arrangements.

4. Model results and discussion

The model described in the previous section was applied to each reactor configuration proposed in this work (reactors A–F) to predict its performance for PCE degradation, and to analyze the effect of the design variables on the pollutant conversion. All the computational simulation results for A–F reactors were obtained with the same operating conditions (see Table 1): inlet volumetric gas flow rate = 100 $cm^3\,s^{-1}$; inlet relative humidity = 50%; PCE inlet concentration = 50 ppm; temperature = 25 °C; pressure = 1 atm; radiation source: Philips TL UV lamp; and 18 W without optical filters. The systems of differential equations were solved by using the finite differences method (with an ad hoc developed FORTRAN program). Details of the numerical procedure are given elsewhere [11].

Fig. 2 shows the predicted values of PCE conversion (Eq. (12)) for each reactor configuration and the partial pollutant conversion achieved in each annular channel for reactors D–F. Exception made for reactor D, the performance of the reactors shows relative improvements on the pollutant conversion when comparing configurations from A to F. It is important to highlight that the predicted improvements can be obtained only by changing the reactor geometry or dimensions, with the same lamp, using the same TiO_2 catalyst and keeping the other operating variables unchanged.

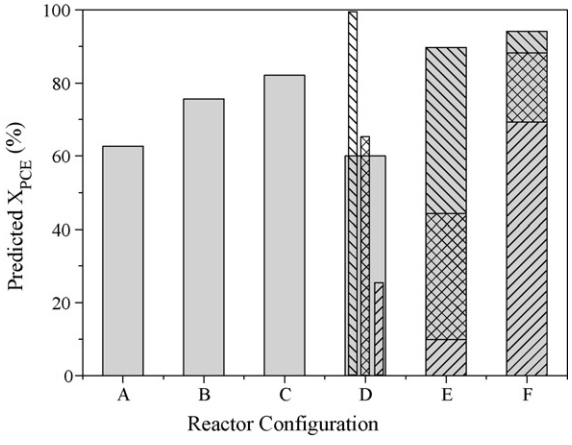

Fig. 2. Predicted values of PCE conversion. Keys: total reactor conversions ( ) and partial conversion in each annular channel: $j = 1$ ( ), $j = 2$ ( ), $j = 3$ ( ).

The values of η_I, η_A, and η_R are predicted with Eqs. (23–25) for the annular reactors in the series A–F are shown in Table 1. The high values of η_I obtained (~82.5%) are characteristic of the annular configuration, due to the geometric compatibility between an annular reactor and a tubular lamp placed at the reactor central axis. The values of η_A are also high, even for the case of single-annular reactors (80.1%, 79.9%, and 77.1% for reactors A, B, and C, respectively). The η_A value increases to 92% when multi-annular reactors D–F are considered. This is a direct consequence of the ability of the multi-annular configuration reactor to absorb most of the radiative energy that have entered it. The photons transmitted by the inner annulus after partial absorption and reflection, can be absorbed by the TiO_2 films of the middle and outer annuli. In contrast to the high values of η_I and η_A, the predicted values of η_R are very low. This result can be understood by considering the much diluted concentration of the pollutant ($C^{in}_{PCE} = 50$ ppm) and the usually low intrinsic efficiency of the photocatalytic reactions. This issue has been discussed in detail elsewhere [23].

Let consider the single-annulus reactors A–C. Although the residence times of reactors B and C (6.3 s and 10.9 s, respectively) are lower than that of reactor A (21.8 s), the predicted values of conversion for both B and C reactors are higher (76.6% for reactor B and 82.1% for reactor C, against 62.7% for reactor A). It should be noted that the values of η_I and η_A corresponding to the three single-annular reactors are almost the same. Thus, neither the reactor radiation incidence efficiency nor the catalyst radiation absorption efficiency is responsible for the differences on the performance among reactors A–C. Nevertheless, it should be noted the concordance between the values of η_R and the values of PCE conversion predicted for reactors A–C (η_R increases with X_{PCE}). As it was observed in a previous work [23], the values of η_R are strongly affected by the external diffusive resistances. To clarify this point, Fig. 3 shows the PCE dimensionless concentration against the radius of the annulus for reactors A–C for different axial positions ($z = 0$, $z = (1/3)Z_R$, $z = (2/3)Z_R$, and $z = Z_R$). As it can be seen from this figure, there are noticeable external concentration radial gradients which indicate the existence of important diffusive resistances. However, the magnitudes of the concentration gradients are not equal in these three reactors, decreasing from reactor A to C.

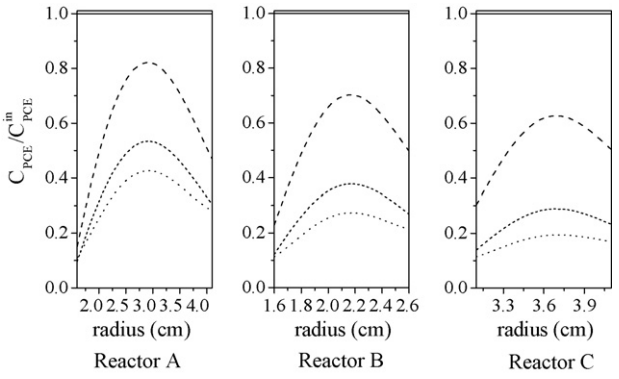

Fig. 3. Dimensionless PCE concentration radial gradients predicted for the following conditions: volumetric flow rate = 100 $cm^3\ s^{-1}$, $C^{in}_{PCE} = 50\ mg\ m^{-3}$, relative humidity = 48%, and SRPA = 1.56×10^{-9} Einstein $cm^{-2}\ s^{-1}$. Keys: (—) $z = 0$, (– – –) $z = 1/3\ Z_R$, (- - -) $z = 2/3\ Z_R$, (···) $z = Z_R$.

The main difference between reactors A and B is the annulus width (2.5 cm and 1 cm, respectively). It can be observed in Fig. 3 that the radial concentration gradient diminishes when the annulus width is smaller. This reduction in the reactant diffusive resistances produces an increment of the PCE conversion of reactor B compared to that of reactor A. Hence, under the employed operating conditions, the reduction in the annulus width improves the reactor performance.

On the other hand, reactors B and C have the same annulus width, but reactor C has a larger photocatalytic surface area. As mentioned before, both reactors B and C absorb approximately the same amount of radiative energy (see η_I and η_A in Table 1). Nevertheless, based on model results, it is possible to conclude that the values of the superficial rate of photon absorption ($e^{a,s}$) are lower on reactor C than on reactor B. By considering the lineal dependence of the $e^{a,s}$ on the rate of PCE degradation (Eq. (15)), it can be concluded that the lower $e^{a,s}$ values will cause lower local reaction rates. The reaction step will control the diffusion-reaction process and the pollutant concentration radial gradient will diminish. Hence, the overall effect of increasing the active photocatalytic area and decreasing the diffusive resistances result in an improvement of the pollutant conversion.

The physically based mathematical model described in the previous section was also used to simulate the performance of the multi-annular reactors D–F. The computer simulation results were obtained adopting the operating conditions of Table 1. As it was previously discussed, reactors D–F have the same dimensions but with differences in either the flow pattern (parallel or series flow operation) or the TiO_2 film thickness. Nonetheless, reactors D–F have the same values of η_I and η_A as shown in Table 1.

It should be noted in Fig. 2 that the multi-annular reactor operating with parallel flow pattern (reactor D) presents the lowest pollutant conversion (60%). Also note that the partial conversions in the inner, middle and outer annular channels are 99.9%, 67% and 25.9%, respectively. The inefficient performance of the outer annular channel is related to the non-uniformity of the LSRPA. By using the mathematical model, it is possible to predict that almost 90% of the useful radiative energy is absorbed on the TiO_2 films of the inner and middle annuli. Therefore, the pollutant degradation takes place mainly in the inner and middle annuli (greater rate of photon absorption), while the PCE conversion produced in the outer annulus is quite low (smaller rate of photon absorption). Besides, from Eq. (7) it may be concluded that the low PCE conversion obtained in reactor D is due to the fact that the pollutant reacts mainly in the inner and middle annuli. The outer annular channel acts as an undesirable by-pass for reactants as a consequence of the lower rate of photon absorption (lower pollutant reaction rate). These results indicate that the multi-annular configuration with parallel flow pattern would be an inefficient alternative for pollutant elimination.

On the other hand, the predicted PCE conversion of reactors E and F are 89.7% and 94.2%, respectively. The values of the intermediate conversion in each annular channel for reactors E and F are shown in Fig. 2. In the same way as reactor D, the PCE

degradation in the reactor E takes place mainly in the inner and middle annuli, and the pollutant conversion in the outer annulus is lower. Nevertheless, the low conversion achieved in the outer annulus (9.9%) is significantly increased after the reactants have flowed through the middle and inner annuli, where the predicted PCE conversion is 44.3% and 89.7%, respectively. From this analysis it is possible to conclude that the series flow pattern (reactors E and F) is more convenient than the parallel flow pattern (reactor D).

From model results, it is possible to conclude that the largest PCE gradients in reactor E are found in the inner annulus channel as a consequence of the highest LSRPA (see Eq. (15)). By reducing the thickness of the TiO_2 film deposited on the walls of the inner annulus and increasing it on the walls of outer annulus, it is possible to modify the photon absorption rate distribution (maintaining the same values of η_I and η_A) and obtain an almost uniform value of LSRPA for all the TiO_2 films (i.e. reactor F). This modification contributes to reduce the diffusive resistances in the inner channel and increases the reaction rate in the middle and outer annuli. The redistribution of the radiative energy achieved by using variable TiO_2 film thicknesses (reactor F) modifies substantially the partial conversion in each annular channel, and improves the overall performance of reactor F.

In this work, we only analyzed the single- and three-annular configurations. A two-annular configuration can also be considered, but the results will be intermediate between the single- and three-annular configurations, closer to the three-annular one.

5. Experimental validation of the model

All the results discussed in the previous section have been obtained by using a predictive model. An essential part of any model development process is the validation of the model predictions by comparing them with experimental data. We chose the multi-annular reactor E (Fig. 1) as the most convenient for model validation purposes because of its good performance for PCE degradation and because it is easier to construct than the other candidate (i.e. reactor F). Therefore, the multi-annular reactor E was constructed with the dimensions shown in Table 1. Previous to the immobilization step, each tube was carefully cleaned first with isopropyl alcohol and then with triple-distilled water. Then, the borosilicate tubes were heated at 500 °C during 5 h to remove any trace of organic compounds that eventually could have been retained on the tubes surface. After the tubes were cooled down to room temperature, each of them was immersed in a aqueous dispersion of TiO_2 particles obtained by using a sol–gel technique [24] and was subsequently withdrawn slowly (3 cm min^{-1}) in order to allow for the liquid in excess to drain. To minimize coating problems related with interface surface tension in the dip-coating process and to improve the uniformity of the TiO_2 films, we added a small amount of a surfactant to the aqueous dispersion of TiO_2 particles. Finally, the tubes were dried in an oven at 80 °C and then heated at 200 °C during 6 h. Experimental and predicted PCE concentrations at the reactor outlet obtained for a chosen range of operating conditions were compared.

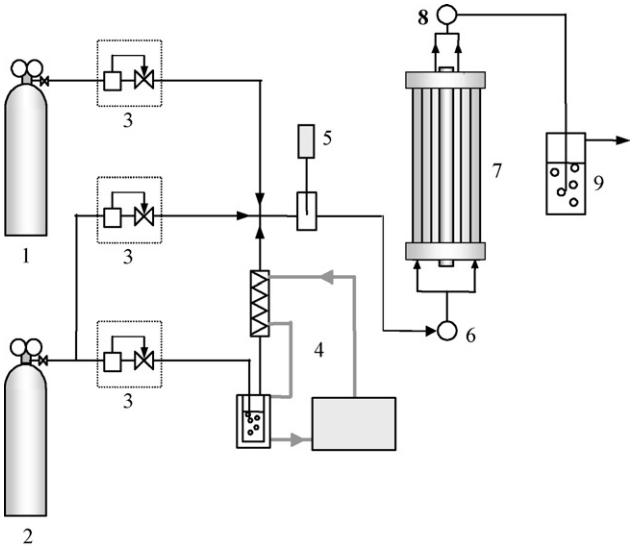

Fig. 4. Flow sheet of the experimental device. Keys: (1) PCE + air; (2) air; (3) mass flowmeters; (4) humidifier system (saturation flask, heat exchanger and thermostatic bath); (5) thermohygrometer; (6) inlet sampling device; (7) photocatalytic reactor; (8) outlet sampling devices; (9) gas scrubber.

The experimental setup employed is schematically shown in Fig. 4. The photocatalytic reactor was fed with a mixture of air, water-saturated air, and PCE-air streams. Pre-established ratios among the mass flows of these three streams allow obtaining a controlled operation, as well as the desired inlet PCE concentration and relative humidity. Chromatographic quality air (air liquide) was used, and the PCE-air mixture was prepared from chromatographic air and liquid PCE (Merck, p.a. quality). The water-saturated air stream was obtained by letting the air stream bubble through a saturation flask containing distillated water at 20 °C. The volumetric flow rates of the three streams (air-PCE, dry air, and water-saturated air) were regulated with on-line mass-flow controllers (Matheson Corp.). The temperature and the relative humidity of the feed stream were measured with an on-line thermohygrometer (Oakton 35612-00) located just upstream from the sampling point in the reactor feed line.

For each experimental run, the operating variables were fixed at the pre-established values, the lamp was turned on, and then the reactor was maintained for 3 h under continuous operation to ensure both constant light intensity and steady state regime of the reaction system. The PCE concentrations in the inlet and outlet streams were measured by off-line gas chromatography (Hewlett Packard 5890; J&W1257032 col.; FID det.). For detecting any possible stable intermediate species and/or reaction by-products, the outlet stream was also analyzed by gas chromatography-mass spectroscopy techniques (Shimadzu QP-5000). The spectral optical properties of the materials employed (glass tubes, TiO_2 films, and neutral filters) were measured with a UV–vis spectrophotometer (Varian Cary, 100 Bio), within the emission wavelength range of the lamp.

The radiation flux reaching the photocatalytic multi-annular reactor was modified by interposing specially constructed

Table 2
Experimental PCE conversions against model predictions[a]

Volumetric flow rate ($cm^3\ s^{-1}$)	Relative humidity (%)	SRPA $\times 10^{-11}$ (Einstein $cm^{-2}\ s^{-1}$)	X_{PCE}^{exp} (%)	X_{PCE}^{mod} (%)	Absolute error (%)
4.17	48	1.00	52.6	40.55	12.05
7.14	48	1.00	30.1	26.26	3.84
12.55	48	1.00	19.1	15.89	3.21
15.82	48	1.00	14.7	12.82	1.88
20.75	48	1.00	11.3	10.00	1.30
12.50	11	1.00	31.7	32.59	0.89
12.50	30	1.00	22.5	21.22	1.28
12.50	48	1.00	19.1	15.92	3.18
12.50	89	1.00	12.9	10.14	2.76
11.36	47	0.79	16.4	14.00	2.40
11.36	47	1.00	23.5	17.46	6.04
11.36	47	2.74	53.8	40.89	12.91
11.36	47	15.00	100	94.38	5.62
11.36	47	26.50	100	99.38	0.62

[a] $C_{PCE}^0 = 50\ mg\ m^{-3}$; $T = 20\ ^\circ C$; $P = 1$ atm.

filters between the lamp and the reactor inner tube. These neutral filters were constructed on red sensitive, 0.1 mm thickness, polyester films, for recorders with He–Ne laser (HNm from AGFA Alliance Recording), by printing different tones of gray with the aid of a software.

Several experimental runs have been performed under different operating conditions (PCE concentration equal to 50 ppm, relative humidity from 10 to 90%, irradiation level from 1.0×10^{-11} to 1.6×10^{-9} Einstein $cm^{-2}\ s^{-1}$, volumetric flow rates from 2 to 30 $cm^3\ s^{-1}$). No degradation of PCE was detected in the absence of either the TiO_2 photocatalyst or UV irradiation. Besides, under the experimental operating conditions, no stable intermediate species and/or reaction by-products were detected by GC-MS. The compounds present in the photocatalytic reactor outlet streams were PCE, H_2O, CO_2, and HCl. Experimental and predicted PCE conversions at the reactor outlet are compared in Table 2. Satisfactory agreement was obtained when experimental and predicted PCE conversions are compared over the entire range of the operating conditions. This is a remarkable result considering that the mathematical model employed in the present work does not make use of any experimentally adjusted parameter.

6. Conclusions

We have studied the performance of six annular photocatalytic wall reactor configurations by using a two-dimensional, reaction-diffusion-convection model and reliable intrinsic reaction kinetics for the photocatalytic degradation of perchloroethylene (PCE). Taking into account that the same model was applied to each one of the six reactors analyzed, for validation purposes we only employed one of the reactors. We chose the multi-annular reactor with its channels interconnected in a series arrangement and uniform TiO_2 film thickness as the most convenient for model validation purposes because of its good performance for PCE degradation. The model was successfully validated against experimental results obtained with this reactor.

Simulation results indicate that:

- Single- and multi-annular photocatalytic reactors present high values of reactor radiation incidence and catalyst radiation absorption efficiencies.
- The performances of the studied reactors are strongly influenced by external diffusive resistances.
- The unfavorable effect of diffusive resistances on the rector performances could be reduced by constructing photocatalytic annular wall reactors of small annular thickness and large irradiated photocatalytic surface areas.
- The multi-annular reactor configuration is very efficient at absorbing most of the radiative energy that have entered it. The photons transmitted by the inner annulus after partial absorption and reflection, can be absorbed by the TiO_2 films of the middle and outer annuli. The multi-annular configuration with parallel flow pattern is predicted to be an inefficient alternative for pollutant elimination.
- The multi-annular reactor with its annuli interconnected in a series pattern, causing the gas stream to reverts its direction when passing from one annulus to the next, is the most adequate among all the studied configurations for PCE photocatalytic elimination.
- The mathematical model developed in this work is a useful tool for the optimal design of a photocatalytic wall reactor.

Acknowledgments

The authors are grateful to Universidad Nacional del Litoral (UNL), Consejo Nacional de Investigaciones Científicas y Técnicas (CONICET), and Agencia Nacional de Promoción Científica y Tecnológica (ANPCyT) for financial support. Thanks are also given to Eng. Gerardo Rintoul for his participation in some parts of the experimental work.

References

[1] M.R. Hoffmann, S.T. Martin, W. Choi, D.W. Bahnemann, Chem. Rev. 95 (1995) 69.
[2] J. Peral, X. Domènech, D.F. Ollis, J. Chem. Technol. Biotechnol. 70 (1997) 117.

[3] D.M. Blake, Bibliography of Work on the Heterogeneous Photocatalytic Removal of Hazardous Compounds from Water and Air, National Renewable Energy Laboratory, Golden, Colorado, 2001.
[4] A. Fujishima, T.N. Rao, D.A. Tryk, J. Photochem. Photobiol. C 1 (2000) 1.
[5] W.A. Jacoby, M.R. Nimlos, D.M. Blake, R.D. Noble, C.A. Koval, Environ. Sci. Technol. 28 (1994) 1661.
[6] R.M. Alberici, W.F. Jardim, Appl. Catal. B: Environ. 14 (1997) 55.
[7] F. Taghipour, M. Mohseni, AIChE J. 51 (2005) 3039.
[8] C.P. Chang, J.N. Chen, M.C. Lu, H.Y. Yang, Chemosphere 58 (2005) 1071.
[9] Y. Ku, K.Y. Tseng, W.Y. Wang, Water Air Soil Pollut. 168 (2005) 313.
[10] F. Shiraishi, D. Ohkubo, K. Toyoda, S. Yamaguchi, Chem. Eng. J. 114 (2005) 153.
[11] G.E. Imoberdorf, A.E. Cassano, O.M. Alfano, H.A. Irazoqui, AIChE J. 52 (2006) 1814.
[12] G.B. Raupp, A. Alexiadis, M. Hossain, R. Changrani, Catal. Today 69 (2001) 41.
[13] C.R. Esterkin, A.C. Negro, O.M. Alfano, A.E. Cassano, AIChE J. 51 (2005) 2298.
[14] S.R.V. Castrillón, H. Ibrahim, H. de Lasa, Chem. Eng. Sci. 61 (2006) 3343.
[15] W.A. Jacoby, D.M. Blake, R.D. Noble, C.A. Koval, J. Catal. 157 (1995) 87.
[16] M. Mohseni, F. Taghipour, Chem. Eng. Sci. 59 (2004) 1601.
[17] G.E. Imoberdorf, H.A. Irazoqui, A.E. Cassano, O.M. Alfano, Ind. Eng. Chem. Res. 44 (2005) 6075.
[18] P.B. Amama, K. Itoh, M. Murabayashi, J. Mol. Catal. A: Chem. 176 (2001) 165.
[19] S. Yamazaki, H. Tsukamoto, K. Araki, T. Tanimura, I. Tejedor-Tejedor, M.A. Anderson, Appl. Catal. B: Environ. 33 (2001) 109.
[20] S. Yamazaki, K. Araki, Electrochemistry 70 (2002) 412.
[21] K.H. Wang, J.M. Jehng, Y.H. Hsieh, C.Y. Chang, J. Hazard. Mater. B90 (2002) 63.
[22] A.E. Cassano, C.A. Martín, R.J. Brandi, O.M. Alfano, Ind. Eng. Chem. Res. 34 (1995) 2155.
[23] G.E. Imoberdorf, A.E. Cassano, O.M. Alfano, H.A. Irazoqui, Chem. Eng. Sci. 64 (2007) 1138.
[24] S. Yamazaki-Nishida, K.J. Nagano, L.A. Phillips, S. Cervera-March, M.A. Anderson, J. Photochem. Photobiol. A 70 (1993) 95.